*

Low-Cost Portable Readout System Design for Inductively Coupled Resonant Sensors

Subhanwit Roy, *Student Member, IEEE*, Yee Jher Chan, Nigel F. Reuel, and Nathan M. Neihart, *Senior Member, IEEE*

***Abstract*— Spiral coil-based LC resonant sensors have seen many applications in agriculture, healthcare, biomanufacturing, and consumer electronics. Traditional techniques to interrogate such sensors using vector network analyzers are expensive and often not portable, whereas custom readouts suffer from either high cost, low range of usable interrogation distances, or low frequency range. This paper proposes a new simple, low-cost, and portable readout design based on the technique of coherent demodulation. A complete theoretical analysis examining how the interrogation distance is related to other circuit parameters is presented. Finally, a complete readout system was implemented using printed circuit board technology and commercially available off-the-shelf components. The system operates between 1-100 MHz and the fabricated system consumes 1.26 W. Measurements show that the system operates reliably and repeatably with interrogation distances up to 5 cm.**

***Index Terms*—Contactless measurement, inductive coupling, interrogation distance, passive wireless LC sensor, readout system, resonance detection, resonant sensor, wireless telemetry**

I. Introduction

As our world undergoes the fourth industrial revolution (Industry 4.0 [1]), fueled by the growth and adoption of smart technologies, there has been a rapid increase in the demand for low-cost, wireless, real-time sensing systems. Spiral coil-based inductor-capacitor (LC) resonators, first used for sensing in 1967 by Collins [2], have emerged as an attractive solution, owing to their passive nature and low-cost fabrication [3]. LC resonant sensors have been demonstrated for a multitude of applications, including pH measurements in bioreactors [4], eye-pressure sensing [5], wound monitoring through bandages [6], measuring the concentration of ionic solutions [7], sweat monitoring in consumer wearables [8], and telemetric measurements at high-temperatures [9]. An extensive survey of papers reporting LC resonant sensors for different applications can be found in [10].

A typical setup to interrogate resonant sensor coils is illustrated in Fig. 1. The signal from the sensor coil is picked up at a distance by the reader coil. Most of the relevant literature uses a vector network analyzer (VNA) to analyze the reflection coefficient spectrum of the reader coil signal and extract information about the sensor's resonance. VNAs are traditionally benchtop equipment costing tens of thousands of dollars, and their capabilities lie way beyond reflection coefficient spectrum analysis. Most of the elaborate capabilities of VNAs that result in increased cost and bulkiness are unnecessary for the sensing applications discussed above, which require a simple, low-cost solution. Moreover, all VNAs require a calibration step before commencing measurement [11], which makes them less attractive for applications that require operation by nontechnical users. Although less expensive and portable alternatives are available [12], [13], they sacrifice accuracy and reliability for cost [14] and often do not offer enough output power or flexible frequency-sweep capabilities to make them conducive for interrogating resonant sensors for different applications. Hence, there is a need for low-cost, portable, compact, robust readout systems for sensing LC resonant sensors that can be easily used by nontechnical personnel.

A practical readout system should be able to read sensors from different interrogation distances (i.e., vertical separation between reader and sensor coils), and the required range of interrogation distances will vary between applications. As changing the interrogation distance affects the coupling coefficient between the reader and sensor coils [15], an additional focus for the readout design would be to build a system with low sensitivity to the variation in coupling coefficient.

While there has been considerable research effort to design LC resonant sensors and make them suitable for different applications, the amount of work put into developing practical readout systems to interrogate such sensors has been disproportionately low [16]. Furthermore, many of the existing custom readout methods, such as exceptional point locking

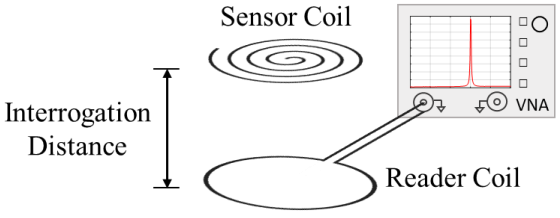

Fig. 1 Traditional setup for interrogating a sensor coil with a reader coil connected to a vector network analyzer. The interrogation distance is the vertical separation between the two coils and it is assumed that there is no horizontal displacement between the centers of the two coils.

Manuscript received December 17, 2021. This work was supported in part by the National Science Foundation under grant number 1827578.

Subhanwit Roy and Nathan M. Neihart are with the Department of Electrical and Computer Engineering, Iowa State University, Ames, IA, 50011 USA.

Yee Jher Chan and Nigel F. Reuel are with the Department of Chemical and Biological Engineering, Iowa State University, Ames, IA, 50011 USA.

[17], diabolic point operation [18], and parity-time symmetric arrangements [19], achieve excellent coupling coefficient sensitivity but require the use of a VNA [20]. Hence, such techniques remain beyond the scope of a low-cost readout design. The prevalent readout techniques for LC resonant sensors that do not require a VNA, or other similar equipment (i.e., impedance analyzer [21], [22], oscilloscope [23], or RF bridge [24]), can be broadly categorized into time-domain and frequency-domain techniques [25].

Time-domain techniques eliminate the need for complicated signal sources by eliminating the need to generate signals over wide frequency ranges [26]. They suffer, however, from the need to have high-resolution test circuits to measure short decay times and small signal amplitudes, increasing the overall cost and complexity of the readout [10]. For these reasons, frequency-domain techniques are much more popular.

Frequency-domain techniques can be further classified as self-oscillating and those which require forced oscillations [20]. Self-oscillating readouts implement the reader coil, which is electromagnetically coupled with the sensor coil, as a part of an oscillator's tank network [27]–[30]. The bias current pulled by the oscillator is affected by the sensor and can be used to extract the sensor's resonant frequency [16]. Also known as a "grid-dip meter," this was the technique used by Collins in 1967 [2]. The grid-dip meter is easy to implement, and the extracted resonant frequency is insensitive to variations in the coupling coefficient. Above a critical coupling coefficient, however, this method exhibits poor phase-noise behavior [16].

Forced oscillation techniques, on the other hand, use an external signal source to generate a frequency sweep excitation of the reader coil. The sensor's resonant frequency is then estimated from the resonant frequency of the reader coil, ω_R, which is typically extracted from the input impedance through either the phase ([31], [32]), the full complex input impedance ([33]–[35]), or the real part ([36]–[40]).

Using the phase of the reader coil's input impedance to estimate the sensor's resonant frequency is heavily dependent on the coupling coefficient, making such readouts susceptible to positional dependence [16]. This makes this method less desirable for hand-held applications, where the interrogation distance cannot be easily maintained.

Measuring the complex impedance of the reader coil, on the other hand, is independent of the coupling coefficient, and therefore does not exhibit such positional dependence [34], [35]. However, as both the real and the imaginary components of the reader coil's input impedance are affected by the sensor in the same way, measuring just one component saves on additional circuitry. Of the two components, measuring the real component results in less complexity and more sensitive to frequency changes near the resonant frequency [36]. Because of this, measuring just the real part of the reader coil's input impedance has become a promising technique. For example, Riistama *et al.* [38] used this to monitor ECG signals around 34 MHz with up to 5.5 cm separation distance between the reader and sensor coil. A summary of the advantages and disadvantages of the different custom readout techniques prevalent in literature that do not require a VNA is provided in Table I.

This paper addresses the gaps in the literature by developing a simple, low-cost readout design platform that can be used to build custom readouts for multiple applications. Informed by existing research, we implement a coherent demodulation technique to detect ω_R, similar to the system architecture presented in [39]. This method is chosen because of its relative simplicity and the fact that ω_R is theoretically independent of the coupling coefficient. However, we made a few significant changes. Firstly, we used a direct digital synthesizer (DDS) as our signal source. Unlike the voltage-controlled oscillator (VCO) of [39], a DDS has a broad output frequency range, a much finer frequency resolution, and almost instantaneous frequency hopping, enabling fast programmable frequency sweeps [31]. Moreover, we replaced the operational transconductance amplifier (OTA) in [39] with an easily customizable common emitter amplifier with emitter degeneration. This change allowed us to eliminate a large DC voltage offset at the input to an analog-to-digital converter (ADC), resulting in an increased dynamic range. Section II provides a complete theoretical analysis of the system, using

TABLE I
SUMMARY OF CUSTOM READOUT TECHNIQUES (NOT REQUIRING A VNA) FOR LC RESONANT SENSORS

Techniques	Advantages	Disadvantages
Time Domain	- Large interrogation distance - Fast measurements due to simple signal source	- Expensive high-resolution test circuits
Frequency Domain – Self Oscillating	- Low-cost - Simple implementation - Large interrogation distance	- Poor phase-noise behavior - Poor sensitivity for large coupling coefficients (small interrogation distances)
Frequency Domain – Forced Oscillations – Phase of Input Impedance Measurement	- Low-cost - Simple implementation	- Extracted resonant frequency is sensitive to coupling coefficient
Frequency Domain – Forced Oscillations – Complex/Real part of Input Impedance Measurement	- Low-cost - Simple implementation - Extracted resonant frequency is theoretically independent of coupling coefficient	- Peak value of real part of input impedance (at resonance) decreases rapidly with a decrease in coupling coefficient

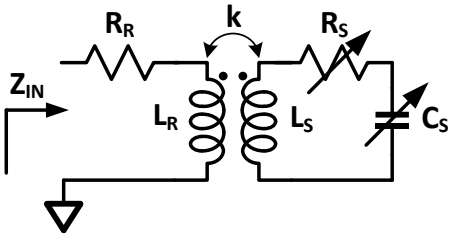

Fig. 2 Lumped circuit equivalent model of sensor and reader coils. L_R and L_S represent the self-inductance of the reader and sensor, respectively, and k is the coupling coefficient between the two coils. The material-under-test is modeled as variable R_S and C_S.

which relevant design tradeoffs are identified. A complete system implementation is described in Section III and experimental results are provided in Section IV. Finally, the paper concludes with Section V.

II. Theory

We start this section by first revisiting, from existing literature, the expression for the input impedance of a reader coil that is inductively coupled to a sensor coil which interacts with a medium-under-test. This expression is then used to find the degrees of freedom for achieving a large interrogation distance. Next, the proposed readout architecture is introduced, and a theoretical analysis of its operation is given. The analysis allows us to identify important design requirements and tradeoffs and sets us up for implementing the readout system in the subsequent section.

A. Input Impedance of An Inductively Coupled LC Resonator

At the core of an LC resonant sensor is a reader coil inductively coupled to a sensor coil that interacts with a medium-under-test. Its equivalent lumped element model is shown in Fig. 2, where L_R and L_S represent the self-inductance of the reader coil and the sensor coil, respectively, and k is the coupling coefficient. The coupling coefficient can be expressed in terms of the mutual inductance M as:

$$k = \frac{M}{\sqrt{L_R L_S}} \tag{1}$$

Further, C_S denotes the capacitance of the medium-under-test, R_S represents losses in the sensor coil and the medium-under-test, and R_R represents the losses in the reader coil. It is assumed that the parasitic capacitance of the reader coil is small enough to be ignored at the frequency range of interest. The equivalent impedance Z_{IN} looking into the reader coil as a function of the angular frequency ω is given by:

$$Z_{IN} = R_R + j\omega L_R \left[1 + \frac{k^2\left(\frac{\omega}{\omega_S}\right)^2}{1+j\frac{1}{Q_S}\left(\frac{\omega}{\omega_S}\right)-\left(\frac{\omega}{\omega_S}\right)^2}\right] \tag{2}$$

where, ω_S and Q_S are the resonant frequency and the quality factor of the sensor, respectively, and are defined as:

$$\omega_S = \frac{1}{\sqrt{L_S C_S}} \tag{3}$$

$$Q_S = \frac{1}{R_S}\sqrt{\frac{L_S}{C_S}} = \frac{\omega_S L_S}{R_S} = \frac{1}{\omega_S C_S R_S} \tag{4}$$

The input impedance Z_{IN} is presented to the readout, which is tasked with measuring ω_S. It has been shown that measuring the real part of Z_{IN} is sufficient for this purpose [16]. Hence, looking at $\mathrm{Re}\{Z_{IN}\}$ in closer detail, we write:

$$\mathrm{Re}\{Z_{IN}(\omega)\} = R_R + L_R k^2 \omega_S Q_S H\left(\frac{\omega}{\omega_S}\right) \tag{5}$$

where

$$H\left(\frac{\omega}{\omega_S}\right) = \frac{\left(\frac{\omega}{\omega_S}\right)^4}{\left(\frac{\omega}{\omega_S}\right)^2 + Q_S^2\left\{\left(\frac{\omega}{\omega_S}\right)^2 - 1\right\}^2} \tag{6}$$

The only part of (5) that changes with ω is $H(\omega/\omega_S)$. In Fig. 3, $H(\omega/\omega_S)$ is plotted for different values of Q_S. It can be observed that $H(\omega/\omega_S)$ has a peak that moves toward ω_S as Q_S is increased. Given the linear relationship between $\mathrm{Re}\{Z_{IN}\}$ and $H(\omega/\omega_S)$ in (5), this peak frequency in $H(\omega/\omega_S)$, corresponds to a peak in $\mathrm{Re}\{Z_{IN}\}$ and can be calculated to be:

$$\omega_R = \frac{2Q_S}{\sqrt{4Q_S^2 - 2}}\omega_S \tag{7}$$

It is evident from (7) that ω_R is independent of the coupling coefficient k and the reader coil circuit parameters. The

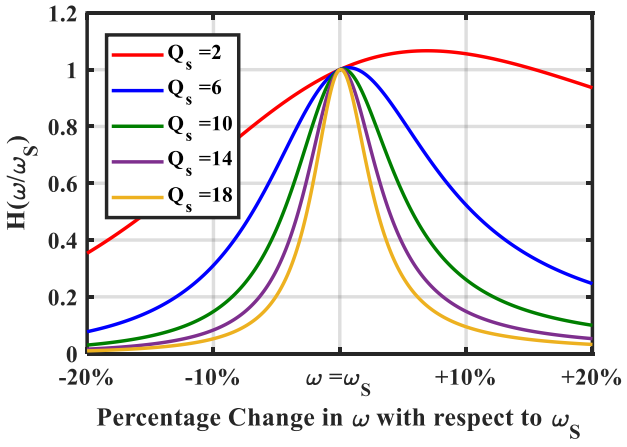

Fig. 3 $H(\omega/\omega_S)$ plotted versus percent change in ω with respect to ω_S. For large Q_S, the frequency where $H(\omega/\omega_S)$ peaks is approximately equal to the sensor resonant frequency, ω_S.

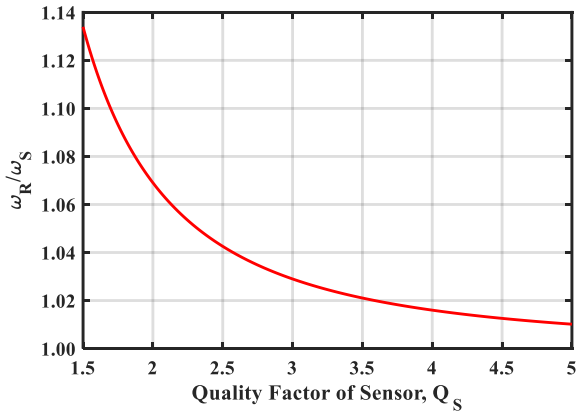

Fig. 4 ω_R/ω_S plotted versus Q_S according to (7). The difference between ω_R andω_S drops below 2% for $Q_S >$ 3.6.

independence of ω_R from k makes the detection of $\mathrm{Re}\{Z_{IN}\}$ a promising candidate for measurements with a large interrogation distance. Also, it can be observed from (7) that for large Q_S, $\omega_R \approx \omega_S$. The plot of ω_R/ω_S versus Q_S, presented in Fig. 4, reveals that the error in approximating ω_S as ω_R drops below 2% for $Q_S > 3.6$. For most practical applications of interest, the resulting quality factor of the sensor would be high enough to make the approximation successfully [10].

Substituting (7) into (5), one can solve for the peak value of $\mathrm{Re}\{Z_{IN}\}$ and arrive at the following approximate equations for the frequency at which $\mathrm{Re}\{Z_{IN}\}$ peaks and the corresponding peak value:

$$\omega_R \approx \omega_S \tag{8}$$

$$\mathrm{Re}\{Z_{IN}\}|_{max} \approx R_R + L_R k^2 \omega_S Q_S \tag{9}$$

Assuming $Q_S > 3.6$, one would want $\mathrm{Re}\{Z_{IN}\}|_{max}$ to be significantly larger than $\mathrm{Re}\{Z_{IN}(\omega)\}$ at frequencies away from resonance. Moreover, it can be seen from (8) and (9) that although the frequency at which $\mathrm{Re}\{Z_{IN}\}$ peaks is independent of the coupling coefficient k. the peak value shows a strong (squared) dependence on k. In fact, according to (5), above a small offset caused by R_R, k^2 scales $\mathrm{Re}\{Z_{IN}\}$ for all ω uniformly. Hence, as the separation between the reader and sensor coils is increased, and k is effectively decreased, the difference between $\mathrm{Re}\{Z_{IN}\}|_{max}$ and $\mathrm{Re}\{Z_{IN}\}$ at frequencies away from resonance decreases rapidly. Thus, given a set of reader and sensor coils and the corresponding readout instrumentation, there will be a limit to the maximum interrogation distance feasible, beyond which the peak in $\mathrm{Re}\{Z_{IN}\}$ would be too small for the readout to detect.

It is of interest to explore what degrees of freedom are available to the designer to compensate for a small coupling coefficient k. In (5), it appears that a decrease in k can be counterbalanced by an increase in L_R, ω_S or Q_S. While the latter two quantities are properties of the medium-under-test and the sensor, and cannot be modified by the designer, increasing the self-inductance L_R of the reader coil can be a viable option. Moreover, changing L_R by modifying the geometric dimensions of the reader coil can lead to an increase in the mutual inductance M for a given sensor coil, which will result in an increase in k for a given interrogation distance [15]. However, increasing L_R would also imply using a larger reader coil with more parasitic capacitance, thus a lower self-resonant frequency. Hence, there is a tradeoff between obtaining a larger peak in $\mathrm{Re}\{Z_{IN}\}$ and the maximum usable frequency of the reader coil when increasing L_R.

B. Analysis of Proposed Architecture

Next, a readout system for detecting the peak in $\mathrm{Re}\{Z_{IN}\}$ is introduced. A behavioral block diagram of the proposed readout system is provided in Fig. 5. The core principle of operation of the readout is motivated by previous works [16], [36], [39] and can be described qualitatively as follows. The circuit passes a frequency-swept current through the reader coil to generate a voltage proportional to Z_{IN} and having the same frequency as the input current. To avoid confusion, we deliberately denote the angular frequency of the current source set externally as Ω_{src} while using ω to represent the continuous angular frequency variable. The reader coil voltage is subsequently mixed with a reference voltage which has the same frequency

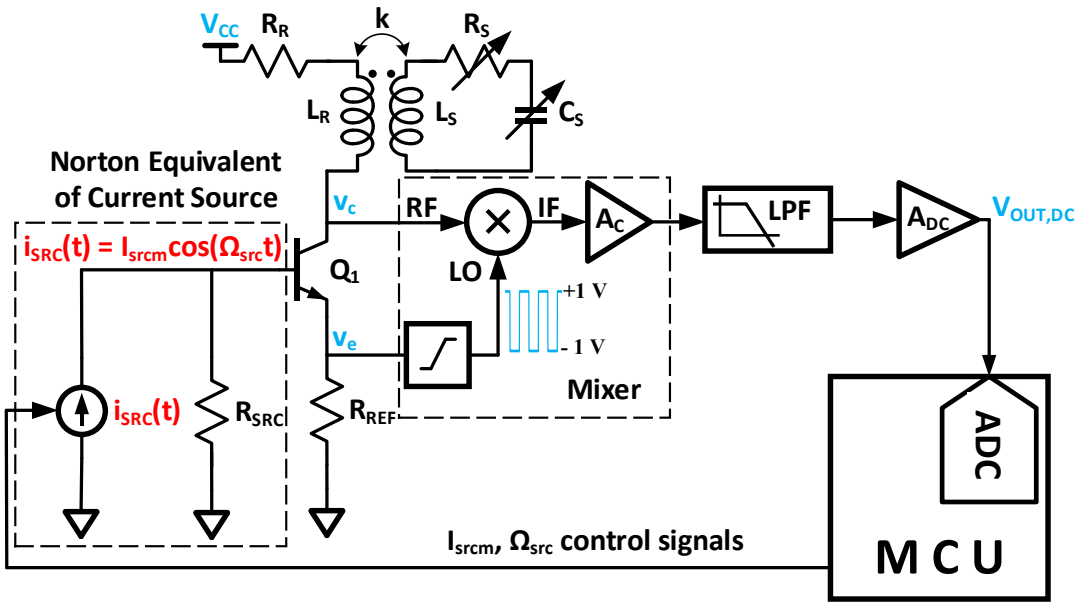

Fig. 5 Block diagram of proposed readout system. A microcontroller unit (MCU) controls the amplitude and frequency of a sinusoidal current source with a time-domain output current $i_{SRC}(t)$ and Norton equivalent resistance R_{SRC}. The emitter voltage, v_e, has the same frequency and phase as the current source, whereas the collector voltage, v_c, has the same frequency but is proportional to the input impedance of the reader coil, Z_{IN}. A mixer, with its LO signal limited to an amplitude of 1 V and a conversion gain A_C, is used to mix the two voltages. The mixer output is then filtered and only the DC component is passed through. This DC voltage is proportional to $\mathrm{Re}\{Z_{IN}\}$ and is amplified before being digitized by an analog-to-digital converter. The frequency of the current source for which $\mathrm{Re}\{Z_{IN}\}$ peaks ($\Omega_{src} = \omega_R \approx \omega_S$) is extracted digitally.

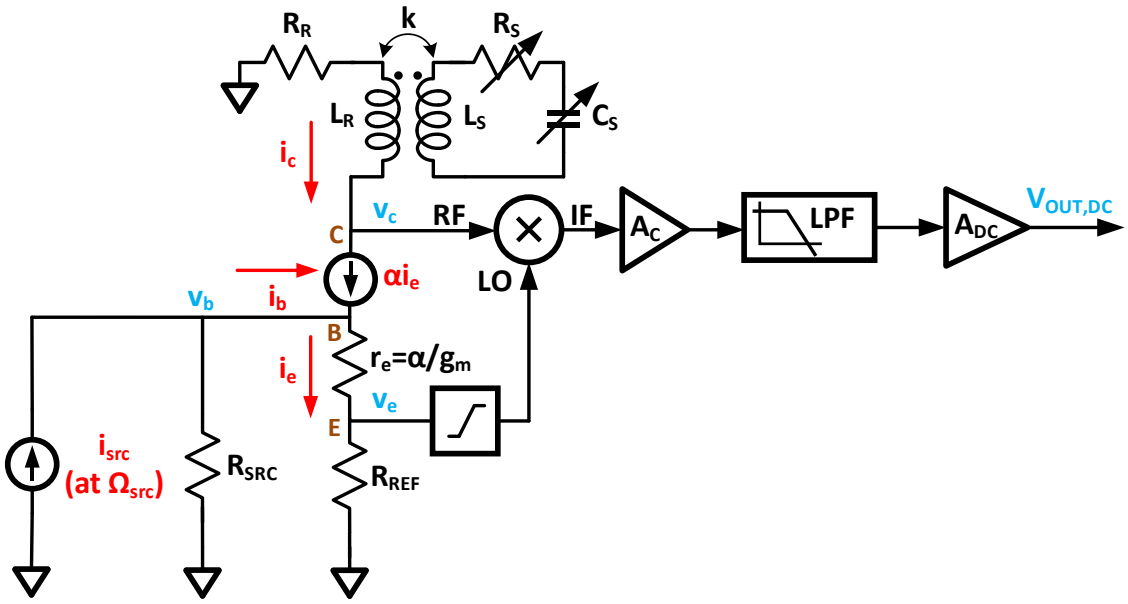

Fig. 6 Equivalent small-signal circuit of the readout circuit. The transistor is replaced by its small-signal T-model. The final output of the system is a DC signal due to the action of the mixer and the lowpass filter.

and phase as the input current. It is assumed that the amplitude of the local-oscillator (LO) input of the mixer is limited (typical of a linear time-variant mixer) to ±1 and the mixer has a conversion gain A_C modeled by the gain block. The coherent demodulation by the mixer results in an output voltage with a DC component proportional to $\mathrm{Re}\{Z_{IN}\}$. To extract this DC component, a lowpass filter is placed at the mixer's output. The filter output is then further amplified by A_{DC} and subsequently sampled by an ADC.

For a more formal description of the readout system, its equivalent small-signal circuit is shown in Fig. 6. To keep the analysis simple, the following assumptions are made. First, it is assumed that the current source produces a sinusoidal current i_{src} with amplitude I_{srcm} and variable angular frequency Ω_{src}. As the AC excursion caused by the input sinusoid would be much smaller than the transistor's DC operating point, the transistor is replaced with its small-signal T-model. Moreover, given that we would operate at frequencies well below 1 GHz where the parasitic capacitances of the transistor would have a very little impact on the transistor's input impedance, we ignore the parasitic capacitances. The Early effect is ignored too as it is not pronounced for discrete transistors. Further, it is assumed that that the mixer is ideal and the LO input is a square wave oscillating between ±1 V. This assumption holds well for linear time-variant mixers where the LO signal amplitude is large enough to completely switch the LO input transistor. Finally, it is assumed that the lowpass filter retains the DC component and filters out all AC components, and the gain block A_{DC} is ideal. These assumptions are reasonable for a lowpass filter with a low enough cutoff frequency to substantially attenuate the lowest frequency AC component in the mixer output (fundamental), and the op-amp used to implement DC gain has large open-loop gain and gain-bandwidth product.

It is important to note that for Figs. 5-6, and the equations to follow, we adopt the following symbol convention. Lowercase symbols with uppercase subscripts denote total instantaneous quantities, whereas uppercase symbols with uppercase subscripts represent DC quantities, and symbols with lowercase subscripts indicate incremental (AC) signal quantities. Phasor quantities are denoted with uppercase symbols and lowercase subscripts with an additional vector sign.

The bulk of the analysis will be carried out in the phasor domain at a generic current source frequency, Ω_{src}. The source can be represented in the phasor domain as:

$$\vec{I}_{src} = I_{srcm}e^{j0} \tag{10}$$

Realizing that this current sees the impedance $R_{SRC}||(\beta+1)(r_e+R_{REF})$, the base voltage is given by:

$$\vec{V}_b = I_{srcm}[R_{SRC}||(\beta+1)(r_e+R_{REF})]e^{j0} \tag{11}$$

Using Ohm's Law at the transistor's base,

$$\vec{I}_e = \frac{I_{srcm}[R_{SRC}||(\beta+1)(r_e+R_{REF})]}{r_e+R_{REF}}e^{j0} \tag{12}$$

Thus, the emitter voltage can be written as:

$$\vec{V}_e = I_{srcm}[R_{SRC}||(\beta+1)(r_e+R_{REF})]\frac{R_{REF}}{r_e+R_{REF}}e^{j0} \tag{13}$$

and the collector current is given by:

$$\vec{I}_c = \alpha\frac{I_{srcm}[R_{SRC}||(\beta+1)(r_e+R_{REF})]}{r_e+R_{REF}}e^{j0} \tag{14}$$

Further, applying Ohm's Law across the reader coil input impedance, Z_{IN}, we can express the collector voltage as:

$$\vec{V}_c = -\alpha\frac{I_{srcm}[R_{SRC}||(\beta+1)(r_e+R_{REF})]}{r_e+R_{REF}}|Z_{IN}|e^{j\theta_{ZIN}} \tag{15}$$

where θ_{ZIN} is the phase of Z_{IN} in radians.

As the mixer operation is better understood in the time-domain, we will convert (13) and (15) to their time-domain representations using the inverse phasor transform at Ω_{src}.

$$v_E(t) = I_{srcm}[R_{SRC}||(\beta+1)(r_e+R_{REF})]\frac{R_{REF}}{r_e+R_{REF}}\cos(\Omega_{src}t) \tag{16}$$

$$v_E(t) = -\alpha I_{srcm}[R_{SRC}||(\beta+1)(r_e+R_{REF})]\frac{|Z_{IN}|}{r_e+R_{REF}}\cos(\Omega_{src}t+\theta_{ZIN}) \tag{17}$$

Due to the action of the ideal limiter, the input to the mixer LO is a square wave given by:

$$v_{LO}(t) = \text{sgn}[\cos(\Omega_{src}t)] \quad (18)$$

Multiplying $v_C(t)$ and $v_{LO}(t)$ in the time-domain and using the Fourier series expansion of (18), the IF output of the mixer can be found to be:

$$v_C(t)v_{LO}(t) = \frac{-\alpha I_{srcm}[R_{SRC}||(\beta+1)(r_e+R_{REF})||Z_{IN}|}{r_e+R_{REF}}\cos(\Omega_{src}t + \theta_{ZIN})\left[\frac{4}{\pi}\cos(\Omega_{src}t) - \frac{4}{3\pi}\cos(3\Omega_{src}t) + \cdots\right] \quad (19)$$

Realizing $\text{Re}\{Z_{IN}\} = |Z_{IN}|\cos(\theta_{ZIN})$, absorbing the factor $-2/\pi$ into the conversion gain of the mixer A_C, and applying the ideal LPF action and a final gain stage of A_{DC}, we obtain:

$$V_{OUT,DC}\big|_{\Omega_{src}} = \frac{\alpha I_{srcm}A_CA_{DC}}{r_e+R_{REF}}[R_{SRC}||(\beta+1)(r_e + R_{REF})]\text{Re}\{Z_{IN}(\omega=\Omega_{src})\} \quad (20)$$

The subscript Ω_{src} is used in conjunction with $V_{OUT,DC}$ to emphasize that the quantity is a DC voltage for a given input current source frequency, Ω_{src}, and is not a sinusoidal voltage with frequency Ω_{src}. Further, approximating α to 1 and assuming $R_{REF} \gg r_e$, (20) can be rewritten as:

$$V_{OUT,DC}\big|_{\Omega_{src}} \approx \frac{I_{srcm}A_CA_{DC}[R_{SRC}||(\beta+1)R_{REF}]\text{Re}\{Z_{IN}(\omega=\Omega_{src})\}}{R_{REF}} \quad (21)$$

It is evident from (20)-(21) that $V_{OUT,DC}\big|_{\Omega_{src}}$ is directly proportional to $\text{Re}\{Z_{IN}(\omega=\Omega_{src})\}$. Hence, when the frequency of the current source Ω_{src} is swept, according to (7) and (8), $V_{OUT,DC}\big|_{\Omega_{src}}$ peaks when $\Omega_{src} = \omega_R$. The DC voltage $V_{OUT,DC}$ can be subsequently digitized over a sweep of Ω_{src} and the peak frequency ω_R, which corresponds to the sensor's resonant frequency ω_S, can be evaluated. To successfully capture the peak in $V_{OUT,DC}$ digitally, it is desirable to have a large difference between $V_{OUT,DC}\big|_{max}$ at ω_R and $V_{OUT,DC}$ at $\omega \neq \omega_R$.

Now, we shall investigate the readout circuit design parameters from (21) and related constraints with the aim of designing a readout system for a large interrogation distance. (21) provides the designer with four degrees of freedom to compensate for the reduction of $\text{Re}\{Z_{IN}\}$ due to a small coupling coefficient k, and the following describes actions that the designer can take to achieve a large interrogation distance.

Firstly, the current source should be chosen to have a large current amplitude I_{srcm} and a large output impedance R_{SRC}. However, a large input swing at the base of the transistor, courtesy of a large I_{srcm} or R_{SRC}, can lead to a large collector voltage swing. If this voltage results in saturating the mixer input, this nonlinear distortion will lead to inaccuracies in peak detection.

Next, the mixer and DC gain stage should provide large gain A_C and A_{DC} respectively. Nevertheless, at large interrogation distances the DC voltage at the mixer output becomes very small and noise starts to play an important role. Any subsequent gain amplifies both the signal and the noise equally and adds its own noise, resulting in limited benefit in peak detection.

Finally, a small value of the emitter degeneration resistance R_{REF} should be chosen. However, R_{REF} has to be large enough for the approximation of $R_{REF} \gg r_e$ made in (21) to hold, the input impedance looking into the base of the transistor to not be sensitive to changes in the current gain β, and meeting the LO input drive requirements of a real mixer. Furthermore, if R_{REF} is not significantly larger than $R_{SRC}/(\beta+1)$, it would decrease the quantity $R_{SRC}||(\beta+1)R_{REF}$ in the numerator of (21), which would be undesirable for large interrogation distances.

III. System Implementation

This section describes the implementation of the readout system shown in Fig. 5 using commercial off-the-shelf components. The readout hardware was implemented on a

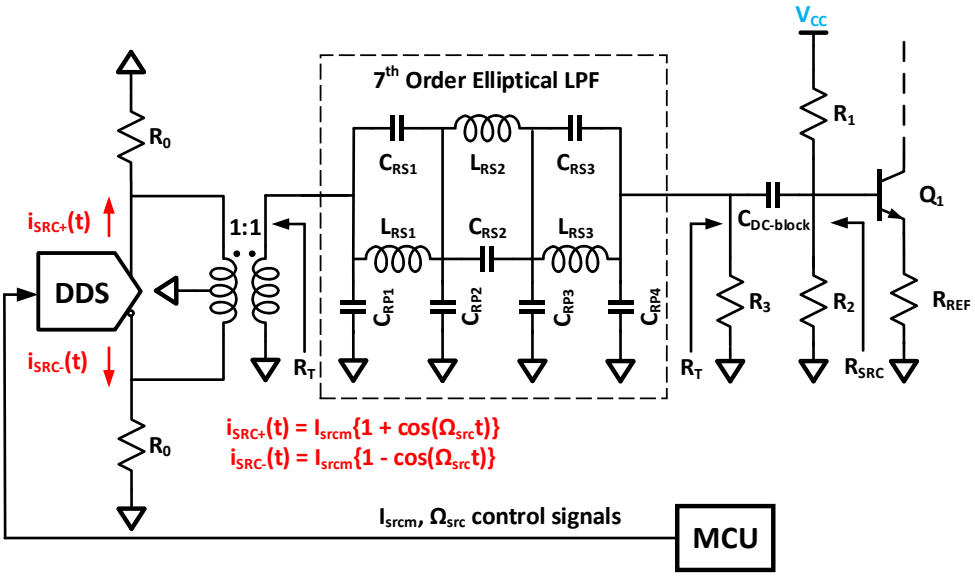

Fig. 7 Detailed schematic of the current source described in Fig. 5. A DDS, controlled by a microcontroller, generates a balanced-output current. Each DDS output is terminated by a resistor, R_0, and a transformer provides the required differential-to-single-ended conversion to drive a low-pass reconstruction filter. The source termination impedance of the filter is determined by R_0 and the transformer, whereas the load termination impedance is determined by the amplifier block.

printed circuit board (PCB), and a microcontroller unit (MCU) was programmed to control the input current source and digitize the readout output. Since many resonant sensing applications target resonant frequencies from a few to tens of MHz [6]–[8], [41], the readout system was built to operate from 1 MHz to 100 MHz. Furthermore, for added modularity, the readout system was designed agnostic of the reader coil to enable the user to utilize coil dimensions targeted to their specific application of interest.

A. Direct Digital Synthesizer Current Source

The readout circuit presented in Fig. 5 requires an easily-controllable AC current source of which the output frequency can be swept over a wide range. A direct digital synthesizer (DDS) emerged as a compelling candidate for this purpose. A DDS produces frequency-tunable analog waveforms by generating a time-varying digital waveform referenced to a fixed-frequency clock and subsequently converting it to its analog form using a digital-to-analog converter (DAC) [42]. Being digital in nature, a DDS renders itself readily to external digital control. Further, it offers extremely fast switching between output frequencies, fine output frequency resolution down to micro-Hz and operation over a wide range of frequencies. Moreover, a DDS is less susceptible to performance degradation due to component aging and temperature drift – factors commonly ailing voltage-controlled oscillator (VCO)-based solutions. From the multitude of DDSs available in the market, the Analog Devices AD9913 was selected for the readout implementation, owing to its low cost, low power, and capability to produce a frequency-agile sinusoidal current of amplitude up to 4.55 mA and frequency up to 100 MHz.

Despite all the above advantages, the output of a DDS has large amounts of harmonic distortion, due to its sampled nature. This necessitates the use of a sharp cut-off reconstruction filter [43].

1) Reconstruction Filter Termination Requirements

The system clock frequency of the AD9913 is 250 MHz and its maximum desired output frequency is 100 MHz. The lowest DAC image will therefore occur at 150 MHz [43]. To pass the desired 100 MHz output signal while sufficiently attenuating the 150 MHz image, a 7th-order low-pass elliptical filter with 100 MHz cutoff frequency was designed [44]. The schematic of the DDS-based current source, including the reconstruction filter, is shown in Fig. 7. A key requirement of this type of filter is the value of the termination impedance, R_T, which must be presented at both the input and output of the filter. It can be seen in Fig. 7 that the value of R_T at the input of the filter is given by [45]:

$$R_T = 2R_0 \tag{22}$$

where R_0 is the termination resistance required by the DDS. At the output of the filter, R_T can be written as:

$$R_T = R_1||R_2||R_3||(\beta+1)(r_e + R_{REF}) \tag{23}$$

where it as assumed that the DC blocking capacitor is an ideal short at the frequencies of interest. Finally, the expression for R_{SRC} in Fig. 7 is given by:

$$R_{SRC} = R_1||R_2||R_3||R_T \tag{24}$$

We can combine (23) and (24) to write:

$$R_T/2 = R_{SRC}||(\beta+1)(r_e + R_{REF}) \tag{25}$$

Now, we previously established that we want $R_{REF} \gg R_{SRC}/(\beta+1)$ to obtain a large value of $V_{OUT,DC}\big|_{\Omega_{src}}$, according to (21). By imposing the same condition on (25), we can write:

$$R_{SRC} \approx R_T/2 = R_0 \tag{26}$$

It is evident from (26) and (21) that for operation at large values of interrogation distance, a reconstruction filter with a large source and load termination R_T would be desired. However, increasing R_T would lead to an increase in the values of L_{RS1}, L_{RS2} and L_{RS3} and an associated reduction in their self-resonant frequencies. Furthermore, a large R_T would necessitate a large R_0, which, for a given value of I_{srcm}, would be limited by the AC compliance voltage rating of the DDS [45]. These two tradeoffs dictated the final choice of R_T for the readout implementation.

Although the reconstruction filter removes harmonics and DAC images, the amplitude of the fundamental signal will follow a $\mathrm{sinc}(\Omega_{src}/\Omega_{clk})$ response over the programmed output frequency [42], where Ω_{clk} denotes the angular system clock frequency of the DDS. For the AD9913, this would result in an amplitude roll-off of 2.42 dB from DC to the maximum output frequency of 100 MHz. Thus, (20) can be recast as:

$$V_{OUT,DC}\big|_{\Omega_{src}} = \frac{\alpha I_{srcm}(\Omega_{src})A_C A_{DC}}{r_e+R_{REF}}[R_{SRC}||(\beta+1)(r_e + R_{REF})]\mathrm{Re}\{Z_{IN}(\omega=\Omega_{src})\} \tag{27}$$

The dependence of I_{srcm} on Ω_{src} would impact the detection of a peak in $\mathrm{Re}\{Z_{IN}\}$ and, thus, would need to be accounted for.

While the variation in current amplitude could be easily corrected through programming the full-scale current of the DDS to compensate the $\mathrm{sinc}(\Omega_{src}/\Omega_{clk})$ roll-off, such a solution would reduce I_{srcm} at lower frequencies from the maximum, an unwanted condition for large interrogation distances. Hence, instead we implement a background correction method to deal with the $\mathrm{sinc}(\Omega_{src}/\Omega_{clk})$ roll off, which will be considered next.

2) Background Correction

Since the dependence of I_{srcm} on Ω_{src} is not affected by the presence of the sensor, it could be captured by measuring the output of only the readout connected to the reader coil with no sensor coil in vicinity. Using (27), the reader-coil-only output, or the "background data" is given by:

$$V_{OUT,DC}\big|_{\Omega_{src}} = \frac{\alpha I_{srcm}(\Omega_{src})A_C A_{DC}[R_{SRC}||(\beta+1)(r_e+R_{REF})]}{r_e+R_{REF}}R_R \tag{28}$$

Dividing (27) by (28), $I_{srcm}(\Omega_{src})$ is eliminated, leaving us with a quantity proportional to $\mathrm{Re}\{Z_{IN}\}$:

$$\frac{V_{OUT,DC}|_{\Omega_{src}}}{V_{OUT,DC}|_{\Omega_{src},background}} = \frac{1}{R_R}\mathrm{Re}\{Z_{IN}(\omega=\Omega_{src})\} \tag{29}$$

As analog division is challenging to implement, the background data is collected and digitized before the start of sensor measurements, and the subsequent division is executed in the digital domain. Finally, the additional step of background correction also enabled the cancelation of any systematic error common to both the background and the sensor data.

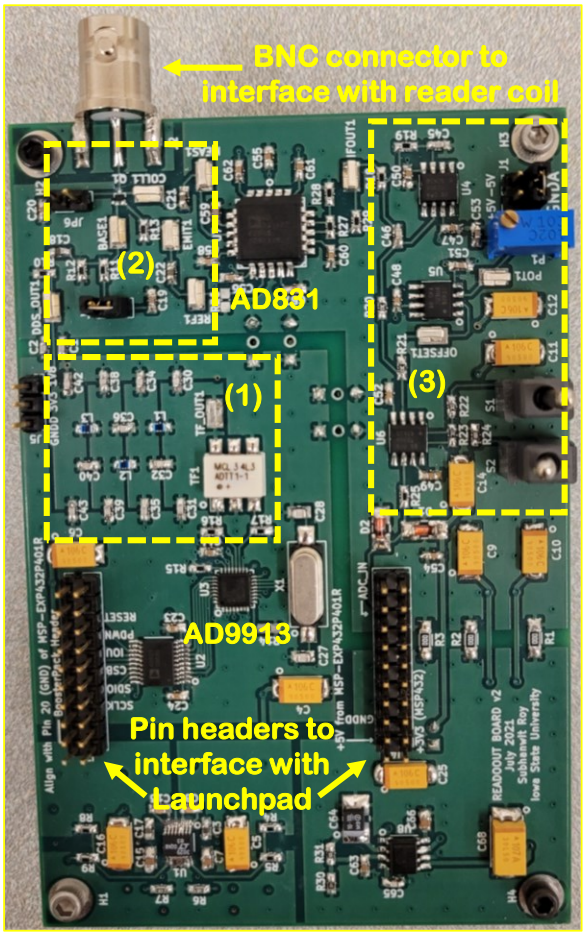

Fig. 8 Photograph of the fabricated readout circuit. The highlighted regions correspond to: (1) the DDS termination network, consisting of transformer and reconstruction filter; (2) the amplifier network, consisting of the BJT, biasing resistors and reference resistor R_{REF}; and (3) the output network, consisting of the LPF and DC gain stage.

TABLE II
ESTIMATED POWER CONSUMPTION BREAKDOWN OF THE FABRICATED READOUT SYSTEM

Readout Block	Power Consumption (mW)	Percentage of Total Power Consumption
DDS	114	9.0%
Amplifier	136	10.8%
Mixer	1,000	79.2%
Output Circuit (LPF + DC Gain)	10	0.8%
ADC	2	0.2%
Total	**1,262**	**100%**

B. Mixer Selection and Amplifier Realization

In the readout system, the mixer facilitates coherent demodulation for signals between 1 to 100 MHz. Based on the required frequency range and the need for a high conversion gain to compensate for low k according to (20), Analog Devices AD831 was selected. It is a double-balanced mixer with a minimum LO input switching level of 200 mVp-p and an input 1 dB compression point of +10 dBm. According to (21), a small R_{REF} is desired for large interrogation distances; however, the minimum LO switching level of the mixer limited the minimum voltage swing of v_e in Fig. 6, thus constraining the smallness of R_{REF}. On the other hand, the linearity specification in the form of the input 1 dB compression point set a limit on the maximum amplitude of v_c in Fig. 6. This is because driving the mixer into compression would make A_C non-constant, leading to inaccuracies in resonant frequency measurement. For most large interrogation distance applications, the mixer's linearity would not affect readout operations as the main challenge would, in fact, be to maintain a high enough v_c in the presence of a low k. However, for an application requiring small reading distances and with a low-loss medium-under-test (high Q_S), linearity could cause a potential issue. In such a scenario, I_{srcm} of the DDS could be reduced.

The amplifier circuit was realized using a BFR380F RF transistor which is highly linear across the frequencies of interest. The resistors R_1 and R_2, in Fig. 7, were sized to provide the required base bias, whereas R_{REF} was chosen to be of the same order of magnitude as R_{SRC}. Further, it was ensured that the output current of the DDS would be able to generate a large enough v_e and fully switch the mixer's LO input.

Finally, a 2nd-order Sallen-Key lowpass filter (LPF) with a cutoff frequency of 10 kHz was implemented to preserve the DC component of the mixer output while attenuating the harmonic components. A non-inverting amplifier followed the LPF to provide user-controlled DC gain and offset.

The reader circuit is controlled using a Texas Instruments MSP432 Launchpad. Furthermore, the ADC of the microcontroller is used to digitize the output signal for subsequent offline digital signal processing to extract the peak frequency.

The readout hardware was implemented on a four-layer PCB with FR4 substrate ($\epsilon_r = 4.1$). The final board is 4" × 3.5". A photograph showing the top view of the final

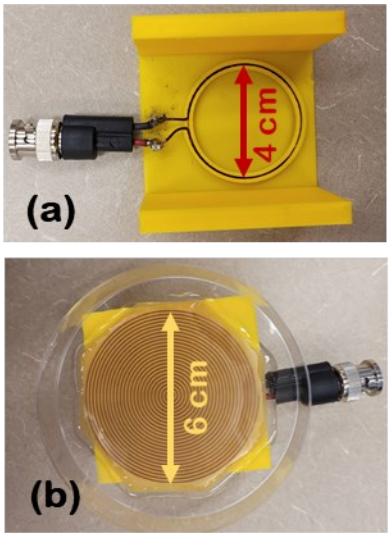

Fig. 9 Photograph of (a) the bottom view of single-turn reader coil placed in custom 3D-printed ABS platform, and (b) the top view of sensor coil adhered to petri dish using epoxy and placed on top of the reader coil platform.

readout board highlighting the key blocks is shown in Fig. 8. Further, Table II lists the estimated power consumption by the different blocks of the implemented readout system.

IV. Experimental Setup and Measurement Results

Having implemented the complete readout system, laboratory experiments were performed to validate its performance.

A. Fabrication of Reader and Sensor Coils

A single 4 cm diameter loop of 18 AWG wire was used for the reader coil and a mold was 3D printed from acrylonitrile butadiene styrene (ABS) plastic to house the reader coil. A BNC connector was soldered to the wire loop to facilitate mating with either the readout board or a VNA. The bottom view of the 3D printed platform with the reader coil and BNC connector is illustrated in Fig. 9 (a).

The sensor coil was designed with 0 cm inner diameter, 6 cm outer diameter, and 0.12 cm pitch and etched using a copper-clad laminate. The fabricated sensor coil was then attached, copper-side down, to a petri dish using epoxy. The top view of the sensor coil, placed on top of the reader coil platform, is shown in Fig. 9 (b). The resonant frequency of the reader-only (with no sensor coil present) was measured to be 144.0 MHz. The resonant frequency dropped to 44.0 MHz when the sensor coil was placed at an interrogation distance of 2 cm.

B. Comparison of Readout with VNA

An Agilent E5071C VNA was used to validate the performance of the low-cost, portable custom readout system in the detection of sensor resonance. The VNA was calibrated from 300 kHz to 100 MHz and then connected to the reader coil. 25 mL of DI water at room temperature was added to the sensor coil petri dish, and the sensor coil was placed at an interrogation distance of 2 cm using a Z-axis positioner. The test setup is shown in Fig. 10. MATLAB was used to extract $\mathrm{Re}\{Z_{IN}\}$, as a function of frequency, from the measured S_{11} and the results are shown in Fig. 11 using the left y-axis.

For measurement with the readout system, first, the reader-only background data was captured, followed by the reader+sensor data. In order to get cleaner peaks, the background data and sensor data had to be individually denoised. For this purpose, we used wavelet denoising as it is has been a common technique to remove noise in image processing applications, and is readily implementable on MATLAB [46]. We employed a sym7 wavelet with 8 levels [47]. A single measurement of the sensor was used as a training dataset (not used in the subsequent validation process) to manually tune the parameters of the Wavelet Denoising algorithm. The denoising method of universal threshold was chosen with soft thresholding and a level-independent noise estimate [46]. After denoising, the sensor data was background-corrected and plotted as a function of the programmed DDS output frequency, Ω_{src}.

Fig. 11 also plots the background corrected and denoised ADC output of the proposed readout system (right y-axis) from 5 MHz to 15 MHz in 20 kHz steps. Notice that the output of the proposed reader aligns nicely with the VNA measurements and both peak at the same frequency (11.0 MHz). This confirms that the readout system responds to $\mathrm{Re}\{Z_{IN}\}$, as described by the analysis. Moreover, the fact that the peak frequency of the custom readout's output is the same as that of a laboratory-grade test equipment demonstrates the effectiveness of the readout in detecting sensor resonance.

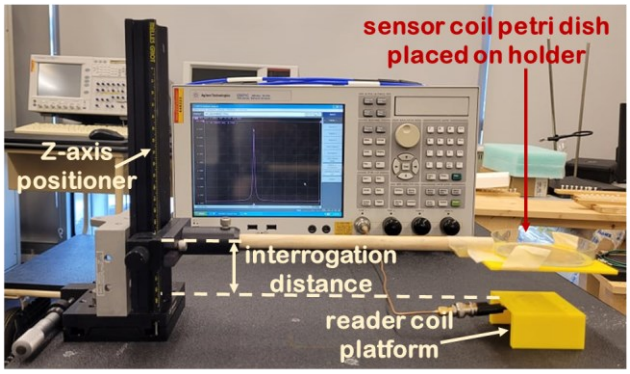

Fig. 10 Photograph of the test setup. The Z-axis positioner is used to control the interrogation distance between the reader and sensor coils. This same setup was used for both VNA characterization of the coils as well as characterization using the proposed readout circuit.

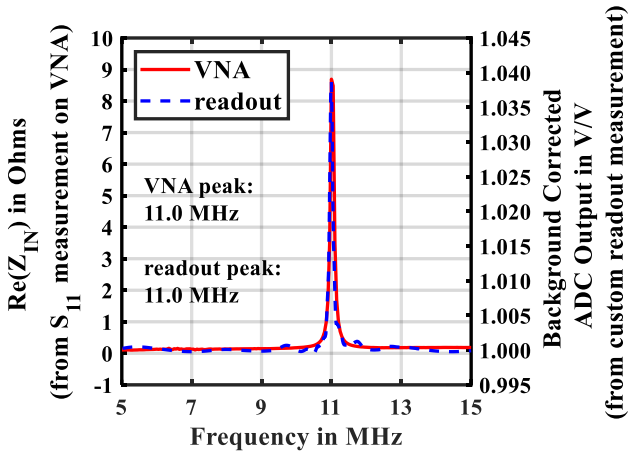

Fig. 11 Comparison of measurements by VNA and custom readout for the sensor coil in room temperature deionized water, with an interrogation distance of 2 cm. The readout data is denoised and background-corrected.

C. Monitoring Temperature Changes in DI Water

The system was then evaluated in a dynamic testing environment. 25 mL of DI water at 65 ºC was added to the sensor coil petri dish and observed for 20 minutes as it cooled down. An Amprobe TMD-56 thermocouple sensor (0.05% basic accuracy) was used to monitor the true temperature of the water, independently, sampling the temperature every minute. Simultaneously, the readout system was programmed to run a periodic frequency sweep from 10.500 MHz to 12.498 MHz with a step size of 2 kHz, once every minute.

MATLAB was used for denoising, background correction and to extract the peak frequency for each measurement by the custom readout system. Peak extraction was done by first computing the mean and standard deviation of the first and last 50 frequency points of each measurement sweep, and then a peak was successfully identified if the maximum output value was larger than 5 standard deviations above the mean.

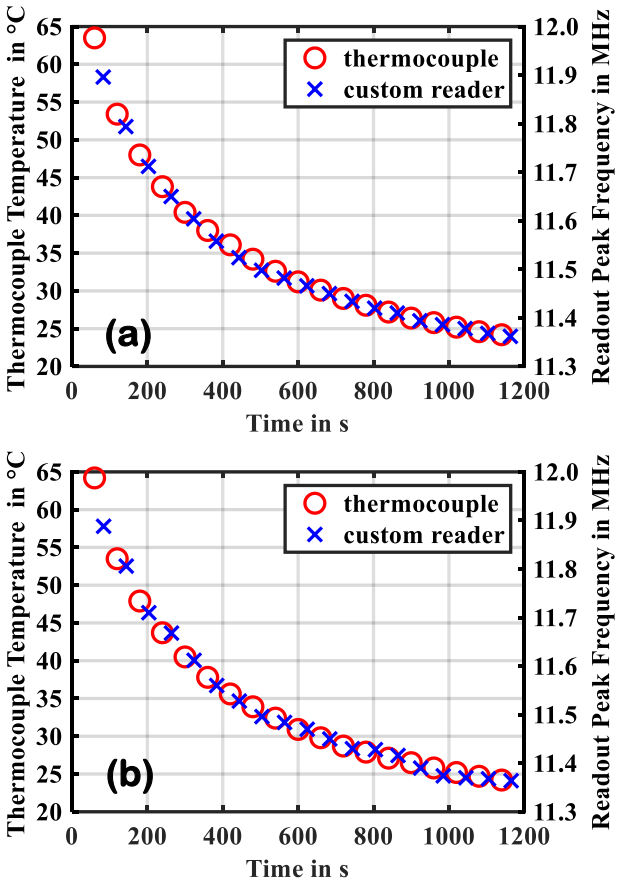

Fig. 12 Comparison of temperature measurement by thermocouple and peak frequency measurement by custom readout for the sensor coil in deionized water at an interrogation distance of (a) 3 cm, and (b) 5 cm. In each case, hot water is added to the sensor coil and measurements are taken as it cools down over time.

The experiment was repeated with interrogation distances from 2, 3, 4, 5, 6, and 7 cm. Results from 3 cm and 5 cm separations are shown in Fig. 12(a) and Fig. 12(b), respectively. In addition, four replicates of the experiment were executed at the interrogation distance of 2 cm to examine the repeatability of the readout system.

Since the two measurement systems were not synchronized to take measurements at the same instant of time, the data points from the thermocouple and the proposed readout do not overlap in time. To make a fair comparison, their outputs were separately interpolated and plotted against each other in Fig. 13. Data from measurements at 2, 3, 4, and 5 cm were used, and the red curve denotes the mean reading, and green bars show the magnitude of errors at distinct frequency points. The maximum error relative to the mean is less than 0.33% pointing to the high insensitivity of the designed readout system over this range of interrogation distances. Furthermore, a straight line fits the mean curve with an R-squared value of 0.99. The linear fit between resonant frequency and temperature is expected as the resonant frequency of an LC resonator has an inverse-square root dependence on the sensing medium's relative permittivity, while a quadratic interpolation can be employed to fit the dependence of DI water's relative permittivity with temperature [48], [49]. Moreover, using the results from the four repetitions of the experiment at the interrogation distance of 2 cm, a similar plot was generated, shown in Fig. 14. The same linear fit to the mean curve, as used in Fig. 13, results in an R-squared value of 0.99. The maximum error relative to the mean is now less than 0.15%, demonstrating excellent repeatability of the readout system.

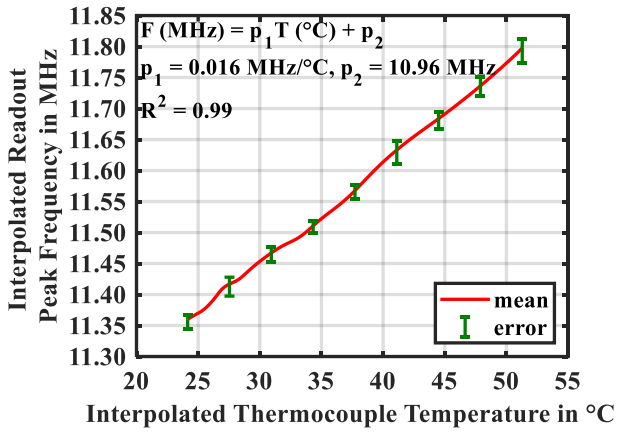

Fig. 13 Interpolated peak frequency from custom readout measurement versus temperature from thermocouple measurement for the sensor coil in deionized water for interrogation distances of 2 cm, 3 cm, 4 cm and 5 cm. The solid red line represents the mean peak frequency for all four interrogation distances at each temperature. The bars show maximum and minimum values of the peak frequency at fixed temperature points. In the fitted equation, F and T denote the readout peak frequency and thermocouple temperature, respectively.

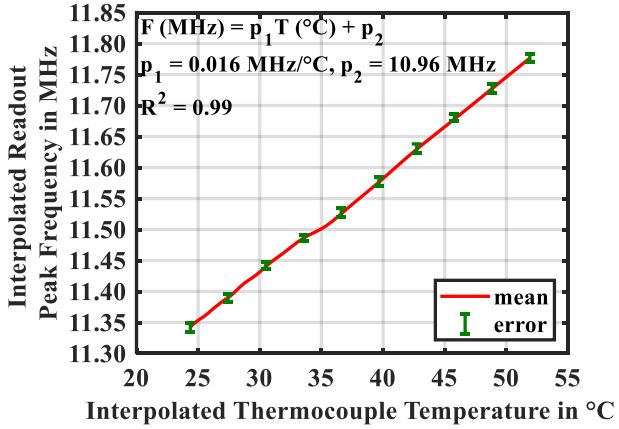

Fig. 14 Interpolated peak frequency from custom readout measurement versus temperature from thermocouple measurements for the sensor coil in deionized water for four separate measurements at an interrogation distance of 2 cm. The solid red line represents the mean peak frequency for all four interrogation distances at each temperature. The bars show maximum and minimum values of the peak frequency at fixed temperature points. In the fitted equation, F and T denote the readout peak frequency and thermocouple temperature, respectively.

It is important to explore the interrogation distance limit of the implemented readout system in the context of the current experiment. Hence, we present the experimental results at large interrogation distances of 6 cm and 7 cm in Figs. 15 (a) and (b) respectively. Although, the readout was able to follow the change in water temperature at an interrogation distance of 6 cm, except at two points, peak detection fails considerably at the interrogation distance of 7 cm. The key performance metrics achieved by the current implementation of the custom readout system are presented in Table III.

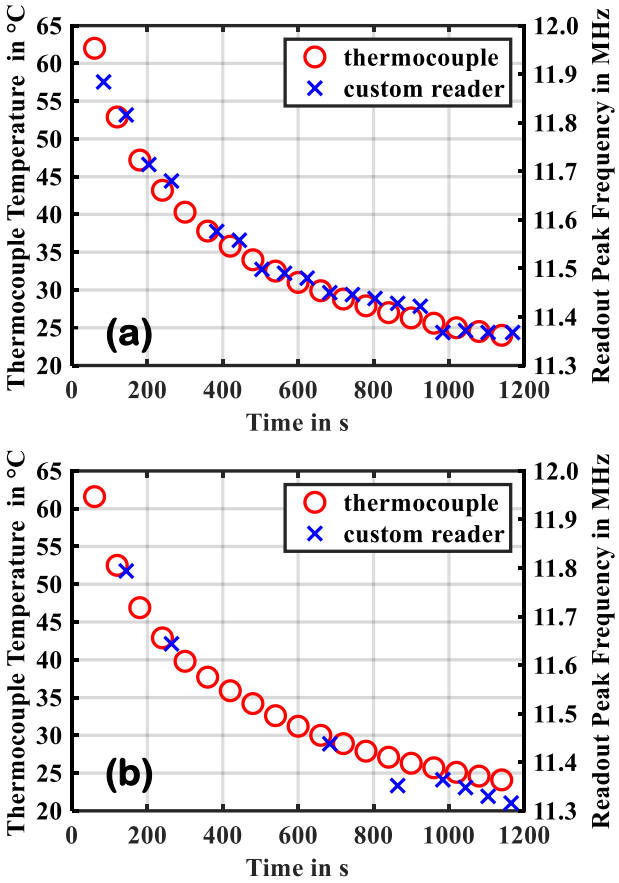

Fig. 15 Comparison of temperature measurement by thermocouple and peak frequency measurement by custom readout for the sensor coil in deionized water at an interrogation distance of (a) 6 cm, and (b) 7 cm. In each case, hot water is added to the sensor coil and measurements are taken as it cools down over time. In (a), the readout is mostly able to track the change in water temperature although it is unable to detect peak at one point and provides a non-monotonic output at another. In (b), the readout is unable to correctly detect most peaks.

TABLE III
KEY PERFORMANCE METRICS ACHIEVED BY IMPLEMENTED READOUT SYSTEM

Performance Metrics	Value
Operating Frequency Range	1-100 MHz
Minimum Frequency Resolution Over Operating Frequency Range	99 kHz
Minimum Frequency Resolution for a 10 MHz Frequency Sweep	10 kHz
Maximum Interrogation Distance (sensor in deionized water)†	5 cm
DC Power Consumption	1,262 mW
Area	14 sq in

†For specific reader and sensor coils used in this paper

Further improvement in the interrogation distance range of the readout could be achieved by using a higher gain setting on the DC amplifier following the output LPF, while an additional enhancement would require a DDS with a higher maximum full-scale DAC output current which would invariably increase the cost of the readout system. Looking beyond the readout system, using a two-loop reader coil to increase the reader-coil self-inductance could be helpful as well. Finally, it should be noted that the achieved range of interrogation distances in the presented experiment would generally not translate to other applications. In particular, the same implementation of the readout system and reader and sensor coils would result in a higher maximum interrogation distance in a sensing medium with lower loss than the one used in the above experiment.

V. CONCLUSION

This paper proposed a new design platform for low-cost portable custom readout systems to interrogate LC resonant sensors wirelessly over varying interrogation distances. The readout was designed to detect sensor resonance by measuring the real part of the input impedance of a reader coil, inductively coupled with a sensor coil, using coherent demodulation. A theoretical analysis led to identifying factors to increase the interrogation distance range and related constraints.

A complete system implementation was then demonstrated, which led to additional requirements and constraints that were discussed accordingly. A complete readout system, having a frequency range of 1-100 MHz, was implemented on printed circuit board technology. The readout hardware used an AD9913 DDS as the signal source and an AD831 mixer for coherent demodulation, while an MSP432 Launchpad was employed to control the hardware and digitize the readout output. The use of the DDS signal source permitted targeting multiple applications over a wide frequency range and enabled fine frequency resolution, fast frequency hopping, and simple programming of frequency sweeps, making the readout easy to use by nontechnical personnel.

Using a set of reader and sensor coils, with the sensor coil placed in deionized water at a 2 cm interrogation distance, we demonstrated an agreement between the readout and a VNA in measuring the sensor resonant frequency. Furthermore, to test the performance of the readout for a dynamic medium-under-test over different interrogation distances, it was used to track the drop in temperature of hot deionized water as it cooled down. The resonant frequency measurements by the readout were compared with independent temperature measurements by a commercial thermocouple probe. A linear fit ($R^2 = 0.99$) between the resonant frequency and temperature data concurred

with the change in the dielectric permittivity of deionized water with temperature. The readout's performance was seen to be repeatable at a fixed interrogation distance (less than 0.15% maximum error relative to the mean using 4 replicates at an interrogation distance of 2 cm) as well as over a range of 2-5 cm (less than 0.33% maximum error relative to the mean using 1 cm steps).

Other researchers and engineers can use the readout design methodology presented in this paper to build custom readout systems targeting specific frequency ranges and interrogation distances for their particular application of interest, thereby replacing expensive VNA-based setups. Future work would involve integrating the microcontroller into the readout board, a more compact board layout, and implementing online signal processing to make the realized readout system ready for industrial/commercial use.

REFERENCES

[1] H. Lasi, P. Fettke, H.-G. Kemper, T. Feld, and M. Hoffmann, "Industry 4.0," *Bus. Inf. Syst. Eng.*, vol. 6, no. 4, pp. 239–242, Aug. 2014, doi: 10.1007/s12599-014-0334-4.

[2] C. C. Collins, "Miniature passive pressure transensor for implanting in the eye," *IEEE Trans. Biomed. Eng.*, vol. BME-14, no. 2, pp. 74–83, Apr. 1967, doi: 10.1109/TBME.1967.4502474.

[3] S. Charkhabi *et al.*, "Effects of fabrication materials and methods on flexible resonant sensor signal quality," *Extreme Mech. Lett.*, vol. 41, p. 101027, Nov. 2020, doi: 10.1016/j.eml.2020.101027.

[4] S. Bhadra *et al.*, "Fluid embeddable coupled coil sensor for wireless pH monitoring in a bioreactor," *IEEE Trans. Instrum. Meas.*, vol. 63, no. 5, pp. 1337–1346, May 2014, doi: 10.1109/TIM.2013.2292279.

[5] P. J. Chen, S. Saati, R. Varma, M. S. Humayun, and Y. C. Tai, "Wireless intraocular pressure sensing using microfabricated minimally invasive flexible-coiled LC sensor implant," *J. Microelectromechanical Syst.*, vol. 19, no. 4, pp. 721–734, Aug. 2010, doi: 10.1109/JMEMS.2010.2049825.

[6] S. Charkhabi, K. J. Jackson, A. M. Beierle, A. R. Carr, E. M. Zellner, and N. F. Reuel, "Monitoring wound health through bandages with passive LC resonant sensors," *ACS Sens.*, vol. 6, no. 1, pp. 111–122, Jan. 2021, doi: 10.1021/acssensors.0c01912.

[7] S. Charkhabi *et al.*, "Resonant sensor arrays for wireless characterization of solvated ions," preprint at https://doi. org/10.26434/chemrxiv 9595628 (2019): v1.

[8] A. R. Carr *et al*., "Sweat monitoring beneath garments using passive, wireless resonant sensors interfaced with laser-ablated microfluidics," *Npj Digit. Med.*, vol. 3, no. 1, pp. 1–9, Apr. 2020, doi: 10.1038/s41746-020-0270-2.

[9] D. Marioli, E. Sardini, and M. Serpelloni, "Passive hybrid MEMS for high-temperature telemetric measurements," *IEEE Trans. Instrum. Meas.*, vol. 59, no. 5, pp. 1353–1361, May 2010, doi: 10.1109/TIM.2009.2038026.

[10] Q. A. Huang, L. Dong, and L. F. Wang, "LC passive wireless sensors toward a wireless sensing platform: status, prospects, and challenges," *J. Microelectromechanical Syst.*, vol. 25, no. 5, pp. 822–841, Oct. 2016, doi: 10.1109/JMEMS.2016.2602298.

[11] A. Rumiantsev and N. Ridler, "VNA calibration," *IEEE Microw. Mag.*, vol. 9, no. 3, pp. 86–99, Jun. 2008, doi: 10.1109/MMM.2008.919925.

[12] "*Metropwr*," Accessed on Dec. 15, 2021. [Online]. Available: https://www.metropwr.com

[13] "*About NanoVNA | NanoVNA*," Accessed on Dec. 15, 2021. [Online]. Available: https://nanovna.com/?page_id=21

[14] N. Ridler and N. Nazoa, *Evaluate accuracy of portable VNAs*, Microwaves & RF, Jan. 15, 2007. Accessed on Dec. 15, 2021. [Online]. Available: https://www.mwrf.com/technologies/test-measurement/article/21841196/evaluate-accuracy-of-portable-vnas

[15] C. M. Zierhofer and E. S. Hochmair, "Geometric approach for coupling enhancement of magnetically coupled coils," *IEEE Trans. Biomed. Eng.*, vol. 43, no. 7, pp. 708–714, Jul. 1996, doi: 10.1109/10.503178.

[16] R. Nopper, R. Niekrawietz, and L. Reindl, "Wireless readout of passive LC sensors," *IEEE Trans. Instrum. Meas*., vol. 59, no. 9, pp. 2450–2457, Sep. 2010, doi: 10.1109/TIM.2009.2032966.

[17] Ş. K. Özdemir, S. Rotter, F. Nori, and L. Yang, "Parity–time symmetry and exceptional points in photonics," *Nat. Mater.*, vol. 18, no. 8, pp. 783–798, Aug. 2019, doi: 10.1038/s41563-019-0304-9.

[18] Z. Dong, Z. Li, F. Yang, C.-W. Qiu, and J. S. Ho, "Sensitive readout of implantable microsensors using a wireless system locked to an exceptional point," *Nat. Electron.*, vol. 2, no. 8, pp. 335–342, Aug. 2019, doi: 10.1038/s41928-019-0284-4.

[19] M. Hajizadegan, M. Sakhdari, S. Liao, and P. Y. Chen, "High-sensitivity wireless displacement sensing enabled by PT-symmetric telemetry," *IEEE Trans. Antennas Propag.*, vol. 67, no. 5, pp. 3445–3449, May 2019, doi: 10.1109/TAP.2019.2905892.

[20] S. Kananian, G. Alexopoulos, and A. Poon, "Coupling-independent sensing systems with fully passive sensors," in *Antenna and Sensor Technologies in Modern Medical Applications*, John Wiley & Sons, Ltd, 2021, pp. 469–521. doi: 10.1002/9781119683285.ch13.

[21] M. Bona, M. Borghetti, E. Sardini, and M. Serpelloni, "Telemetric technique for passive resistive sensors based on impedance real part measurement at fixed frequency," *IEEE Trans. Instrum. Meas.*, vol. 67, no. 9, pp. 2160–2168, Sep. 2018, doi: 10.1109/TIM.2018.2811279.

[22] M. Demori, M. Baù, M. Ferrari, and V. Ferrari, "Electronic technique and circuit topology for accurate distance-independent contactless readout of passive LC sensors," *AEU - Int. J. Electron. Commun.*, vol. 92, pp. 82–85, Aug. 2018, doi: 10.1016/j.aeue.2018.05.019.

[23] Md. R. R. Khan, T. K. An, and H. S. Lee, "A battery-free, chipless, highly sensitive LC pressure sensor tag using PEDOT: PSS and melamine foam," *IEEE Sens. J.*, vol. 21, no. 2, pp. 2184–2193, Jan. 2021, doi: 10.1109/JSEN.2020.3021076.

[24] B. Lin, Q. Tan, G. Zhang, L. Zhang, Y. Wang, and J. Xiong, "Temperature and pressure composite measurement system based on wireless passive LC sensor," *IEEE Trans. Instrum. Meas.*, vol. 70, pp. 1–11, 2021, doi: 10.1109/TIM.2020.3031157.

[25] S. Sauer, U. Marschner, B. Adolphi, B. Clasbrummel, and W.-J. Fischer, "Passive wireless resonant Galfenol sensor for osteosynthesis plate bending measurement," *IEEE Sens. J.*, vol. 12, no. 5, pp. 1226–1233, May 2012, doi: 10.1109/JSEN.2011.2167747.

[26] A. Babu and B. George, "A linear and high sensitive interfacing scheme for wireless passive LC sensors," *IEEE Sens. J.*, vol. 16, no. 23, pp. 8608–8616, Dec. 2016, doi: 10.1109/JSEN.2016.2614816.

[27] J. Coosemans, M. Catrysse, and R. Puers, "A readout circuit for an intra-ocular pressure sensor," *Sens. Actuators Phys.*, vol. 110, no. 1, pp. 432–438, Feb. 2004, doi: 10.1016/j.sna.2003.09.015.

[28] M. Nowak, N. Delorme, E. Colinet, G. Jacquemod, and F. Conseil, "A readout circuit for remote interrogation of capacitance transducers," in *2nd European Conference Exhibition on Integration Issues of Miniaturized Systems - MOMS, MOEMS, ICS and Electronic Components*, Apr. 2008, pp. 1–8.

[29] P. Escobedo *et al.*, "Compact readout system for chipless passive LC tags and its application for humidity monitoring," *Sens. Actuators Phys.*, vol. 280, pp. 287–294, Sep. 2018, doi: 10.1016/j.sna.2018.07.040.

[30] M. A. Carvajal, P. Escobedo, A. Martínez-Olmos, and A. J. Palma, "Readout circuit with improved sensitivity for contactless LC sensing tags," *IEEE Sens. J.*, vol. 20, no. 2, pp. 885–891, Jan. 2020, doi: 10.1109/JSEN.2019.2943002.

[31] T. Salpavaara, J. Verho, P. Kumpulainen, and J. Lekkala, "Readout methods for an inductively coupled resonance sensor used in pressure garment application," *Sens. Actuators Phys.*, vol. 172, no. 1, pp. 109–116, Dec. 2011, doi: 10.1016/j.sna.2011.02.051.

[32] K. Bao *et al.*, "A readout circuit for wireless passive LC sensors and its application for gastrointestinal monitoring," *Meas. Sci. Technol.*, vol. 25, no. 8, p. 085104, Jul. 2014, doi: 10.1088/0957-0233/25/8/085104.

[33] H. S. Kim, S. Sivaramakrishnan, A. S. Sezen, and R. Rajamani, "A novel real-time capacitance estimation methodology for battery-less wireless sensor systems," *IEEE Sens. J.*, vol. 10, no. 10, pp. 1647–1657, Oct. 2010, doi: 10.1109/JSEN.2010.2046407.

[34] E. Sardini and M. Serpelloni, "Wireless measurement electronics for passive temperature sensor," *IEEE Trans. Instrum. Meas.*, vol. 61, no. 9, pp. 2354–2361, Sep. 2012, doi: 10.1109/TIM.2012.2199189.

[35] P. Muthuvel, B. George, and G. A. Ramadass, "A highly sensitive in-line oil wear debris sensor based on passive wireless LC sensing," *IEEE Sens.*

J., vol. 21, no. 5, pp. 6888–6896, Mar. 2021, doi: 10.1109/JSEN.2020.3036154.
[36] S. Lizon-Martinez, R. Giannetti, J. L. Rodriguez-Marrero, and B. Tellini, "Design of a system for continuous intraocular pressure monitoring," *IEEE Trans. Instrum. Meas.*, vol. 54, no. 4, pp. 1534–1540, Aug. 2005, doi: 10.1109/TIM.2005.851216.
[37] Sajeeda and T. J. Kaiser, "Passive telemetric readout system," *IEEE Sens. J.*, vol. 6, no. 5, pp. 1340–1345, Oct. 2006, doi: 10.1109/JSEN.2006.881395.
[38] J. Riistama, E. Aittokallio, J. Verho, and J. Lekkala, "Totally passive wireless biopotential measurement sensor by utilizing inductively coupled resonance circuits," *Sens. Actuators Phys.*, vol. 157, no. 2, pp. 313–321, Feb. 2010, doi: 10.1016/j.sna.2009.11.038.
[39] R. Nopper, R. Has, and L. Reindl, "A wireless sensor readout system—circuit concept, simulation, and accuracy," *IEEE Trans. Instrum. Meas.*, vol. 60, no. 8, pp. 2976–2983, Aug. 2011, doi: 10.1109/TIM.2011.2122110.
[40] W. S. Lee, Y. Kim, and V. Raghunathan, "TeleProbe: zero-power contactless probing for implantable medical devices," in *Proceedings of the 2016 International Symposium on Low Power Electronics and Design*, New York, NY, USA, Aug. 2016, pp. 28–33. doi: 10.1145/2934583.2934593.
[41] S. Charkhabi, A. M. Beierle, M. D. McDaniel, and N. F. Reuel, "Resonant sensors for low-cost, contact-free measurement of hydrolytic enzyme activity in closed systems," *ACS Sens.*, vol. 3, no. 8, pp. 1489–1498, Aug. 2018, doi: 10.1021/acssensors.8b00267.
[42] Ken Gentile and Rick Cushing, *A technical tutorial on digital signal synthesis*, Analog Devices, 1999. Accessed on Dec. 15, 2021. [Online]. Available: https://www.analog.com/en/education/education-library/technical-tutorial-dds.html
[43] W. Kester, "What the Nyquist Criterion Means to Your Sampled Data System Design." Analog Devices, 2008.
[44] D. Brandon and K. Gentile, "DDS-Based Clock Jitter Performance vs. DAC Reconstruction Filter Performance." Analog Devices, 2006.
[45] K. Gentile, "Driving a Center-Tapped Transformer with a Balanced Current-Output DAC." Analog Devices, 2007.
[46] "*Wavelet signal denoising - MATLAB wdenoise*," Mathworks. Accessed on Dec. 15, 2021. [Online]. Available: https://www.mathworks.com/help/wavelet/ref/wdenoise.html#d123e120756
[47] "*Choose a Wavelet - MATLAB & Simulink*," Mathworks. Accessed on Dec. 15, 2021. [Online]. Available: https://www.mathworks.com/help/wavelet/gs/choose-a-wavelet.html
[48] I. M. Hodge and C. A. Angell, "The relative permittivity of supercooled water," *J. Chem. Phys.*, vol. 68, no. 4, pp. 1363–1368, Feb. 1978, doi: 10.1063/1.435955.
[49] A. P. Gregory and R. N. Clarke, *Tables of the complex permittivity of dielectric reference liquids at frequencies up to 5 GHz*, NPL Report, Jan. 2012. Accessed on Dec. 15, 2021. [Online]. Available: https://eprintspublications.npl.co.uk/4347/

Subhanwit Roy (S'18) received his B.Tech. degree in Electronics and Communication Engineering from National Institute of Technology - Durgapur, India, in 2015, and his M.S. degree in Electrical Engineering from Iowa State University, Ames, in 2017. Since 2018, he has been pursuing his Ph.D. degree at Iowa State University. His research interests lie in RF circuit design for next generation wireless communication and sensing technologies, and engineering education.

Yee Jher Chan received his B.S. degree in Chemical Engineering from Iowa State University, Ames, in 2018. He is currently pursuing his Ph.D. degree at Iowa State University in Chemical Engineering. His research focuses on sensor development for agricultural and biological systems.

Nigel F. Reuel received a B.S. degree in Chemical Engineering at Brigham Young University, Provo, in 2009. He received a Ph.D. degree in Chemical Engineering from the Massachusetts Institute of Technology in 2014. In 2016 he joined Iowa State University, Ames, where he is now and Associate Professor of Chemical and Biological Engineering. His research interests center on sensor development for closed systems such as biomanufacturing, agriculture, and wearable technology.

Nathan M. Neihart (M'09—SM'14) received both the B.S. and M.S. degrees in Electrical and Computer Engineering from the University of Utah, Salt Lake City, in 2004. He received the Ph.D. degree in Electrical Engineering from the University of Washington, Seattle, in 2008. In 2008 he joined Iowa State University, Ames, where he is now an Associate Professor in the Dept. of Electrical and Computer Engineering. His research interests include reconfigurable RF circuits and systems for multi-band/multi-mode radios and circuits and systems for sensing applications. From 2010 to 2012 and again from 2016 to 2019, Dr. Neihart served as an Associate Editor for the IEEE Transactions on Circuits and Systems-II: Express Briefs and from 2012 to 2014 as an Associate Editor for the IEEE Transactions on Circuits and Systems-I: Regular Papers.